V European Conference on Computational Fluid Dynamics
ECCOMAS CFD 2010
J. C. F. Pereira and A. Sequeira (Eds)
Lisbon, Portugal,14-17 June 2010

A 3D HUMAN CAROTID ARTERY SIMULATION USING REALISTIC GEOMETRY AND EXPERIMENTAL INPUT DATA

Senol Piskin*, Erke Aribas* and M. Serdar Celebi*

*Istanbul Technical University, Informatics Institute, Computational Science and Engineering,
Ayazaga Kampusu Maslak 34469 Istanbul, Turkey
e-mail: {senol,aribas}@be.itu.edu.tr, mscelebi@itu.edu.tr

Key words: Carotid Artery Bifurcation, Blood Flow, Womersley Velocity Profile, Computational Fluid Dynamics, CFD, Biomechanics, Computed Tomography, CT, Simulation

Abstract. *In this study the biomechanical characteristics of a realistic carotid artery[1] are studied numerically using different inlet velocity profiles. Sinusoidal and several experimental data measured [5] at the common carotid artery are used as inlet boundary conditions . Computation domain is generated using a computed tomography (CT) data of a real patient. Three dimensional (3D) transient NS equations are solved in this actual domain using the proposed boundary conditions. Effects of different input conditions on the results of the simulation are discussed. Main parameters investigated at the critical parts of the carotid artery such as bifurcation and sinusoidal enlargement regions are velocity profiles, wall shear stress (WSS) and pressure distributions. Results show that the input boundary conditions and slope/curtavute discontinuities in the geometry affect the velocity, pressure and WSS distributions highly.*

1 INTRODUCTION

Blood flow in human arteries is a special area of interest because of its importance. It is important since the majority of people in developed countries die because of heart attacks or some other diseases related to blood flow [3]. Atherosclerosis or heart stroke are two fatal disease examples related to the blood flow.

The atherosclerosis affects the flow of blood. This effect, at carotid artery bifurcation may be vital. The atherosclerosis affects millions of people worldwide, leading to such diseases as heart break and stroke [7]. Complex hemodynamics play a critical role in the development of atherosclerosis, the process of aging and many other disease processes. Bio-fluid mechanics play a major role in the cardiovascular system so, it is important to understand the forces and movement of blood cells and whole blood as well as the interaction between the blood cells and the vessel wall [4]. According to the study of Liepsch, D. [4], viscosity and flow behaviour change specifically the creation of vortices, and flow disturbances can be used to show how medication can influence flow behaviour. Experiments have shown that hemodynamics may have a strong influence on the creation of aneurysms and varicose veins. Thus, health care practitioners must understand fluid dynamic factors such as flow rate ratio, pressure and velocity gradients, flow behavior, velocity distribution, and shear stress on the wall and on blood cells. These mechanical factors are largely responsible for the deposit of the cells and lipids which is a leading cause of atherosclerosis. The interaction between blood cells and of the cells with the vessel may cause the formation of plaques and agglomerations. These deposits are found predominantly at arterial bends and bifurcations where blood flow is disturbed, and secondary flows are developed, and flow separation regions are found.

In this paper, the biomechanical properties of flow at carotid artery are investigated. Some characteristic behaviours of blood flow and the relation between the flow inlet at the common carotid artery and the flow properties throughout the artery are analyzed.

2 GEOMETRIC RECONSTRUCTION

All sliced images from a patient are used as the input. These images are gathered on top of each other to form the 3D design. Filtering carotid artery sections from this group of images leads to structuring a geometric model which is created as a surface, consuming triangle cells (Figure 1). However, in order to simulate a flow model, geometry has to be filled with volumetric cells. This step is achieved by using a 3D volume meshing tool. Refinements and smoothing methods are used to obtain a volume mesh with a good quality of skewness.

Geometry of the carotid artery including level 2 branching is shown in Figure 2

3 WOMERSLEY VELOCITY PROFILE

The velocity inlet profile is taken as Womersley velocity profile which is used by [6] and [8]. But for all time steps, the profiles were approximated to parabolic velocity profiles by

Figure 1: Selecting blood vessels from the CT data of a patient.

Figure 2: Actual carotid artery geometry taken from a patient

assigning the maximum velocity of the Womersley velocity profile as the maximum velocity of the parabolic velocity profile. The flow rate data are the same with the data used in [2]. The velocity inlet boundary condition at the common carotid artery is evaluated by the following equation which is given in [6]:

$$u_z(r,t) = \text{Real}\left(\frac{-j\alpha(w)}{w}e^{jwt}\left[1 - \frac{J_0\left(\sqrt{-j}W_0\frac{r}{R}\right)}{J_0\left(\sqrt{-j}W_0\right)}\right]\right), \tag{1}$$

where $u_z = u_z(r,t)$ is the axial velocity, r the radial coordinate, J_0 is the Bessel function of order zero and $W_0 = R\left(wr/\nu\right)^{1/2}$ the Womersley number. The Womersley number is a non-dimensional parameter which can be interpreted as the ratio of the unsteady forces to the viscous forces [3].

The Womersley velocity profile for the axial component of velocity, $w(r,t)$ in terms of the flow rate data at the input is then given by

$$w(r,t) = \frac{2B_0}{\pi R^2}\left[1 - \left(\frac{r}{R}\right)^2\right] + \sum_{n=1}^{N}\left[\frac{B_n}{\pi R^2}\left[\frac{1 - \frac{J_0\left(\alpha_n\frac{r}{R}j^{3/2}\right)}{J_0\left(\alpha_n j^{3/2}\right)}}{1 - \frac{2J_1\left(\alpha_n i^{3/2}\right)}{\alpha_n j^{3/2}J_0\left(\alpha_n j^{3/2}\right)}}\right]\right] \tag{2}$$

Our carotid artery model entrance is very close to an ellipse in shape. So, the womersley velocity profile is interpolated (approximated) to an elliptic paraboloid velocity profile. The ratio of minor radius to major radius is 7/8. Thus, the eccentricity of the ellips is about 0.484.

The shape of elliptic paraboloid for a sample time step is shown in Figure 3.

The flow rate data used to obtain the velocity profile is shown in Figure 4 for two cardiac cycles.

4 FLOW MODEL

3D Navier-Stokes equations are used as the governing equations of blood flow (3). Energy equation is not included in the governing equations since the effect of temperature change is relatively small. Blood is assumed as a Newtonian fluid and the density is taken as constant throughout the domain and time.

$$\begin{aligned}
\text{div}\mathbf{u} &= 0 \\
\rho\frac{\partial u}{\partial t} + \text{div}(\rho u\mathbf{u}) &= -\frac{\partial p}{\partial x} + \text{div}(\mu grad u) + 0 \\
\rho\frac{\partial v}{\partial t} + \text{div}(\rho v\mathbf{u}) &= -\frac{\partial p}{\partial y} + \text{div}(\mu grad v) - g \\
\rho\frac{\partial w}{\partial t} + \text{div}(\rho w\mathbf{u}) &= -\frac{\partial p}{\partial z} + \text{div}(\mu grad w) + 0
\end{aligned} \tag{3}$$

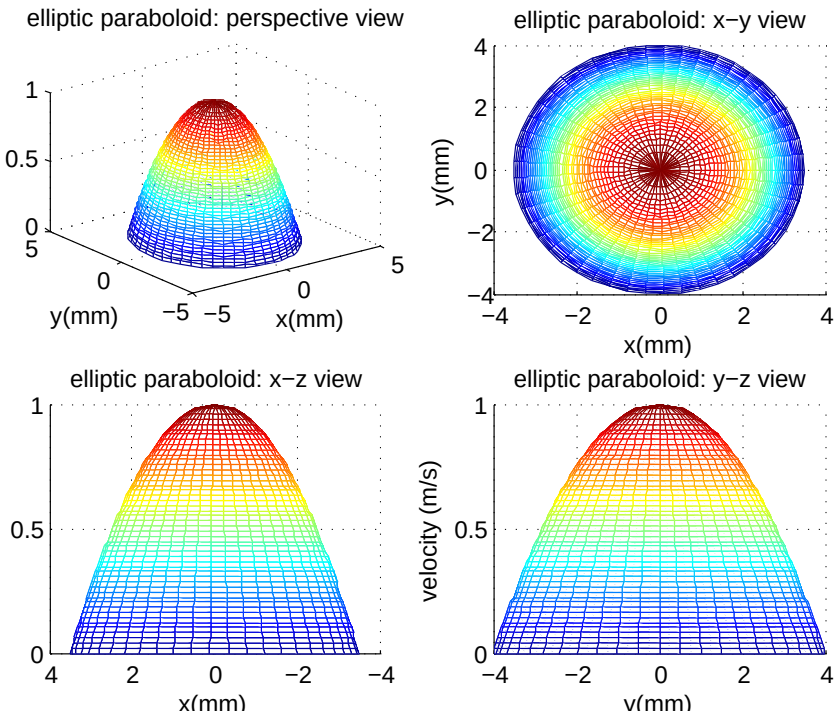

Figure 3: Eliptic paraboloid shape used as input to carotid artery model.

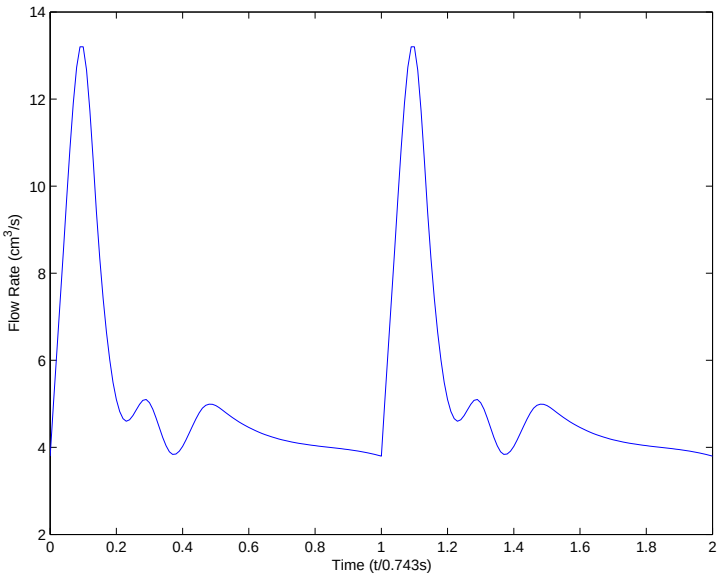

Figure 4: The physiological flow rate in the carotid artery for two cardiac cycles. The unit of flow rate is cm^3/s and the time is dimensionless (dividing real time by one cardiac cycle time: 0.743 second.)

Both steady and unsteady blood flows are simulated. In the steady flow simulation, the boundary conditions are chosen as in the middle of diastole. In the unsteady flow, the physiological waveform was taken as the inlet velocity boundary condition at common carotid artery and the results of steady flow simulation are taken as initial conditions for unsteady flow simulation.

5 INPUT PROFILES

Several input profiles are used in this study. One of them is the sinusoidal input data which is obtained from maximum and minimum values of the experimental data and it is shown in Figure 5. Other profiles are obtained using experimental data. These profiles are presented in Figures 6(a), 6(b), 6(c), and 6(d).

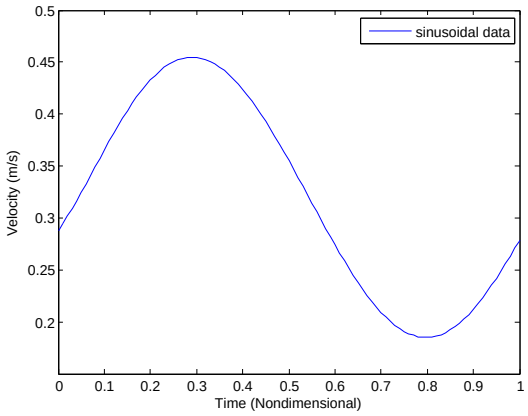

Figure 5: Sinusoidal velocity data

All of the four experimental based input data are shown in Figure 7.

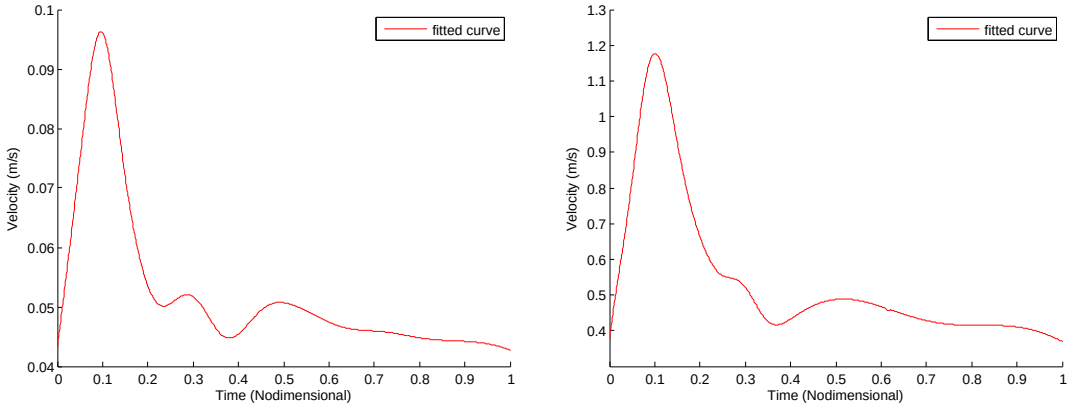

(a)

(b)

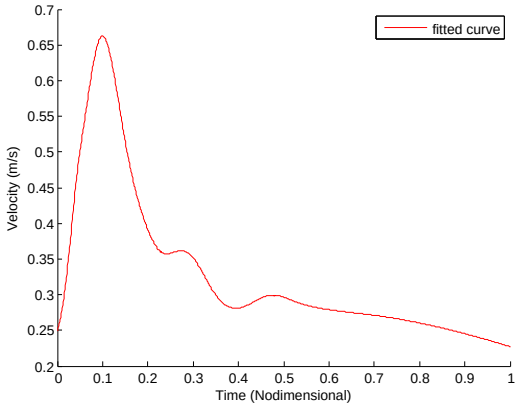

(c)

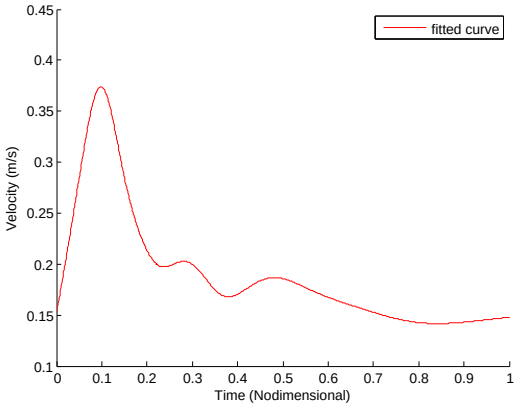

(d)

Figure 6: The inlet velocity data at the common carotid artery for one cardiac cycle. The unit of flow is are meter per second and the time is given in dimensionless form (by dividing real time by one cardiac cycle time: 0.743 second). Cases have different velocity magnitudes as shown in the figures a) Case 1, b) Case 2, c) Case 3, d) Case 4.

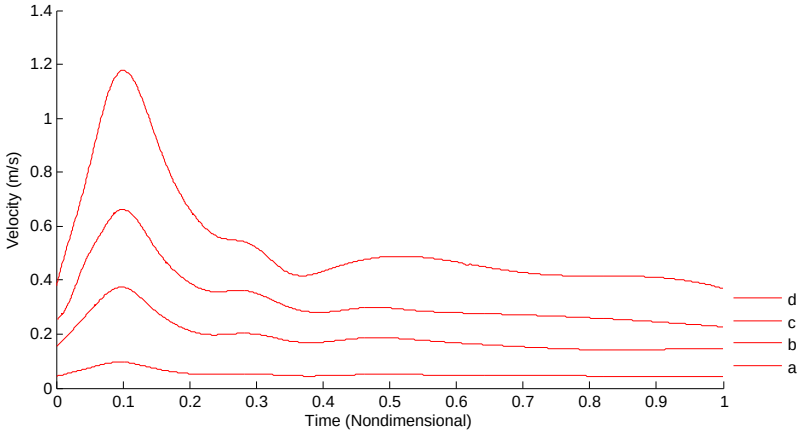

Figure 7: All inlet velocity data at the common carotid artery for one cardiac cycle

6 RESULTS

Figures 10, 11, and, 12 show the velocity, pressure and wall shear stress values for the low velocity inlet case (case a) at the six selected points respectively. It can be seen from Figure 10 that points 3 and 5 have the lowest velocity histories. This is mainly because of the enlargement at the sinus region of the internal carotid artery. Point 3 has lower velocity history than the point 5 because of the low velocity near non-divider wall at the bifurcation area. Points 4 and 6 have the highest velocity histories because of the stenosis and the relatively high blood flow rate into the internal carotid artery. For this relatively low velocity inlet, the pressure histories at the six points are very close to each other in shape and magnitude. This is not surprising since this is the total pressure and the effect of the velocity into this value is relatively small. This can be verified by very low pressure values (around zero) at points 4 and 6 where the velocity have the highest values. The stenosis region (points 4 and 6) have the highest wall shear stress history. This result is suitable with the theory that the plaque rupture is related with high wall shear stress.

When the velocity inlet has higher values (case-d), points 4 and 6 have the highest velocity histories while the points 2 and 3 have the lowest velocity histories as can be seen in Figures 13, 14, and, 15. In this case, point 5 has higher velocity history than that of the point 2. Also the velocity history at point 3 for case-d has lower magnitude values for some time interval than that of the case-a while the inlet profile has higher velocity

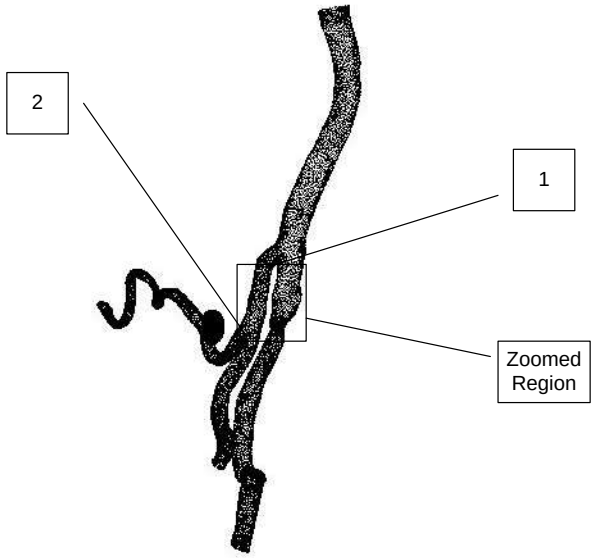

Figure 8: L f the first two points

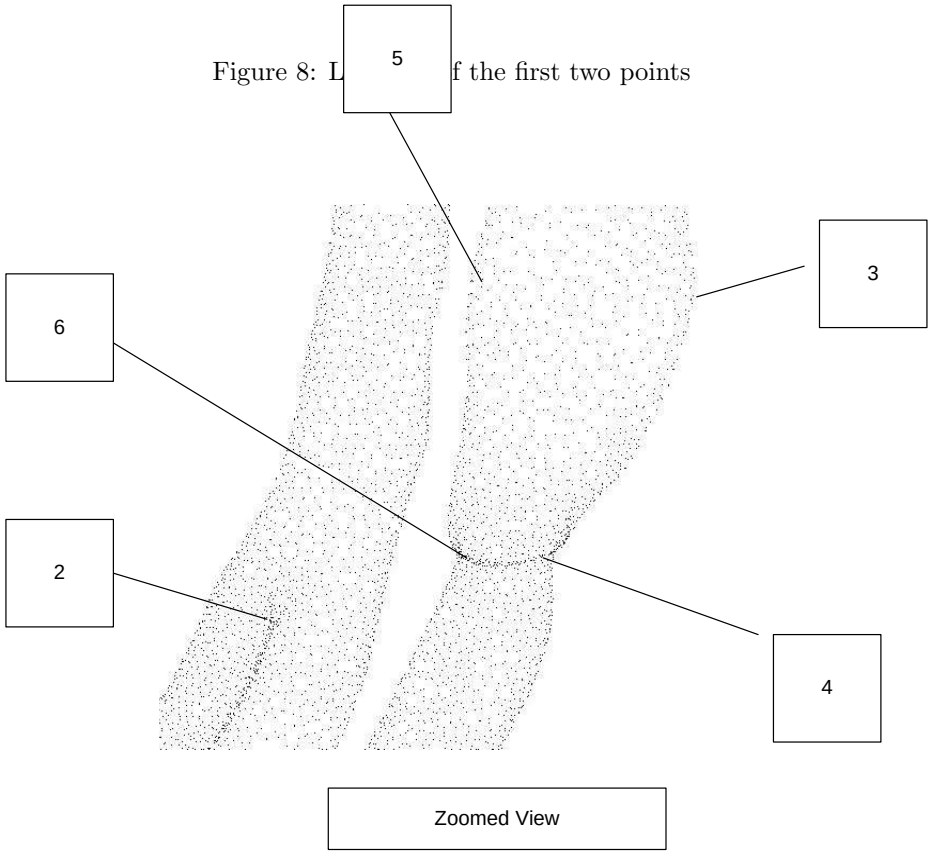

Figure 9: Figure showing the locations of the points

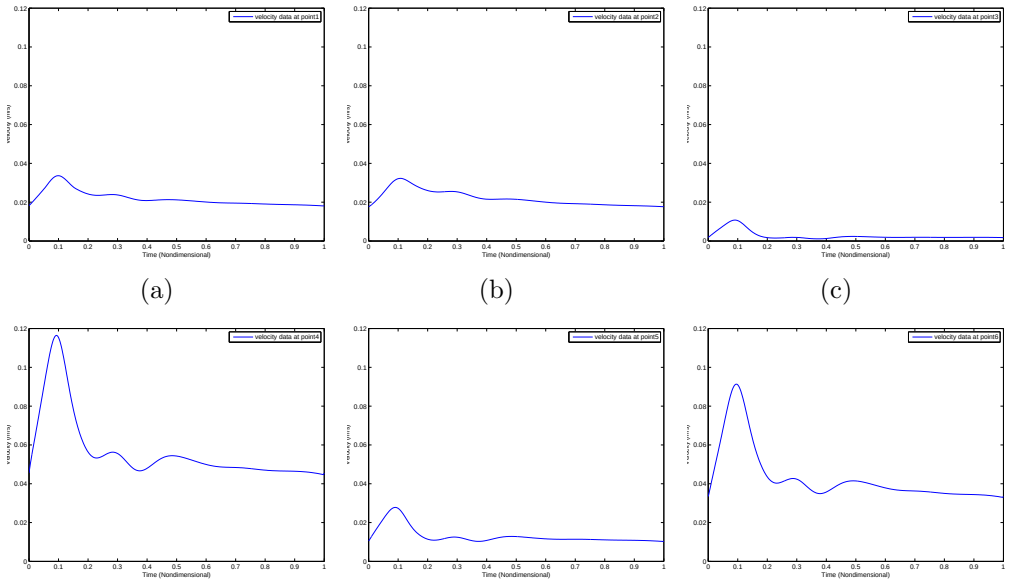

(a) (b) (c)

(d) (e) (f)

Figure 10: The velocity data at the selected six points for one cardiac cycle. The unit of velocity is m/s and the time is given in dimensionless form (by dividing real time by one cardiac cycle time: 0.743 second). Points have different velocity values as shown in the figures a) Point 1, b) Point 2, c) Point 3, d) Point 4, e) Point 5, f) Point 6.

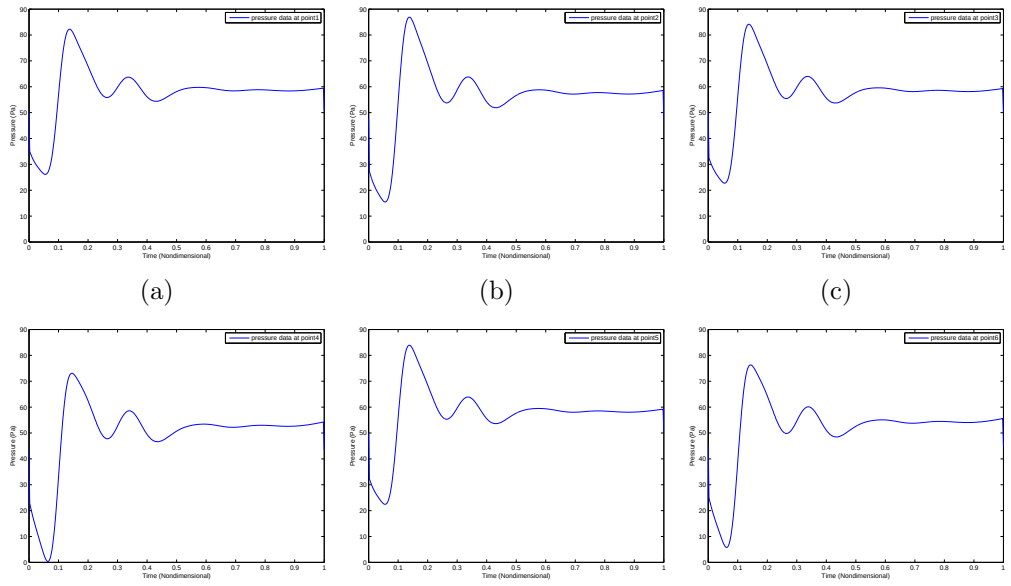

(a) (b) (c)

(d) (e) (f)

Figure 11: The pressure data at the selected six points for one cardiac cycle. The unit of pressure is Pa and the time is given in dimensionless form (by dividing real time by one cardiac cycle time: 0.743 second). Points have different pressure values as shown in the figures a) Point 1, b) Point 2, c) Point 3, d) Point 4, e) Point 5, f) Point 6.

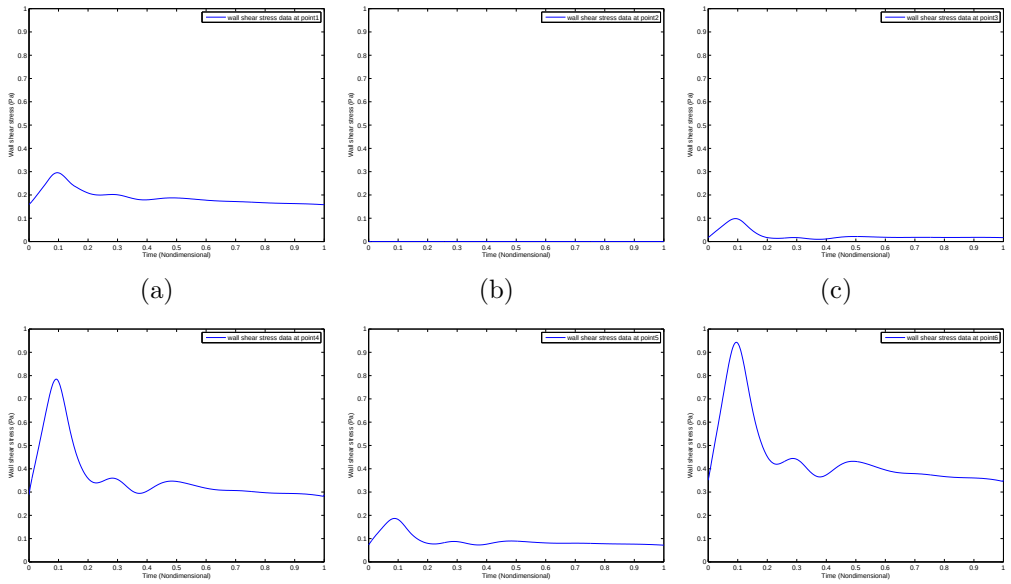

(a) (b) (c)

(d) (e) (f)

Figure 12: The wall shear stress data at the selected six points for one cardiac cycle. The unit of wall shear stress is Pa and the time is given in dimensionless form (by dividing real time by one cardiac cycle time: 0.743 second). Points have different wall shear stress values as shown in the figures a) Point 1, b) Point 2, c) Point 3, d) Point 4, e) Point 5, f) Point 6.

values at that time interval for case-d. These show that the inlet velocity magnitude changes the relative magnitude of the values at the points (for example at point 3). It may be caused because of developement of vortex or of secondary flow. Shape of the velocity history at point 3 is different from the shape of the inlet velocity data while other points have similar shape. This verifies the nonlinear relations (vortex, secondary flow etc.). Pressure histories at points 4 and 6 show sharp drop at time 0.1 which is not seen in case-a. This is the result of very high velocity at points 4 and 6 for case-d. Relation between developement of plaque and high wall shear stress can be verified with the results of the case-d also. It should also be mentioned that the shape of the WSS history at point 3 is different from those at other points. This is again the result of nonlinear relations.

Figure 16 shows the velocity histories at point 1 for all cases together. The shapes of these historical data are very different while the velocity profiles have similar shapes (Figure 6). This results show that the mechanical properties of the blood flow depend not only at the shape of the velocity inlet data but also at the magnitude of the inlet data. The dependence on the magnitude is very strong and nonlinear. Similar differences can be seen in pressure history values too (Figure 17).

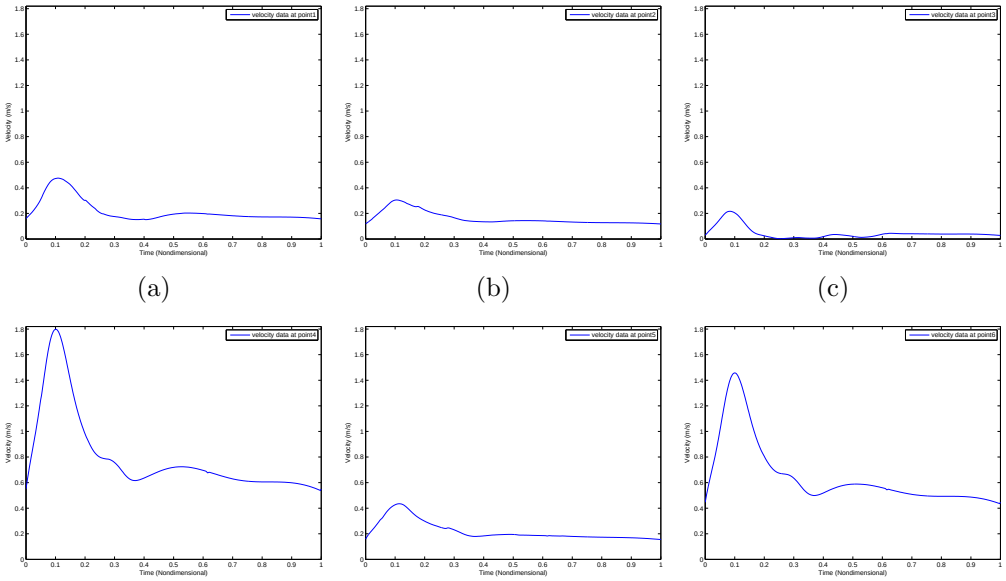

(a) (b) (c)

(d) (e) (f)

Figure 13: The velocity data at the selected six points for one cardiac cycle. The unit of velocity is m/s and the time is given in dimensionless form (by dividing real time by one cardiac cycle time: 0.743 second). Points have different velocity values as shown in the figures a) Point 1, b) Point 2, c) Point 3, d) Point 4, e) Point 5, f) Point 6.

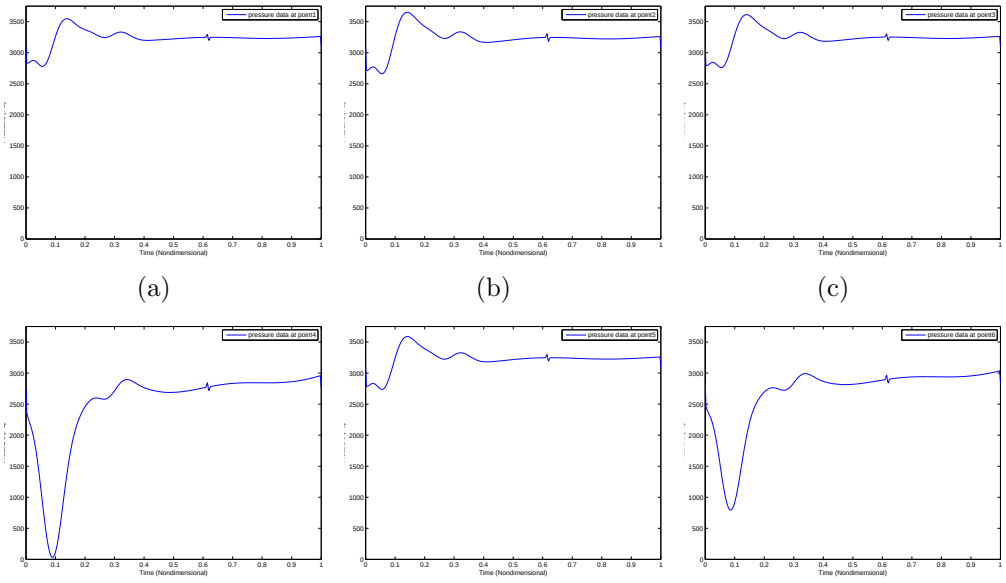

(a) (b) (c)

(d) (e) (f)

Figure 14: The pressure data at the selected six points for one cardiac cycle. The unit of pressure is Pa and the time is given in dimensionless form (by dividing real time by one cardiac cycle time: 0.743 second). Points have different pressure values as shown in the figures a) Point 1, b) Point 2, c) Point 3, d) Point 4, e) Point 5, f) Point 6.

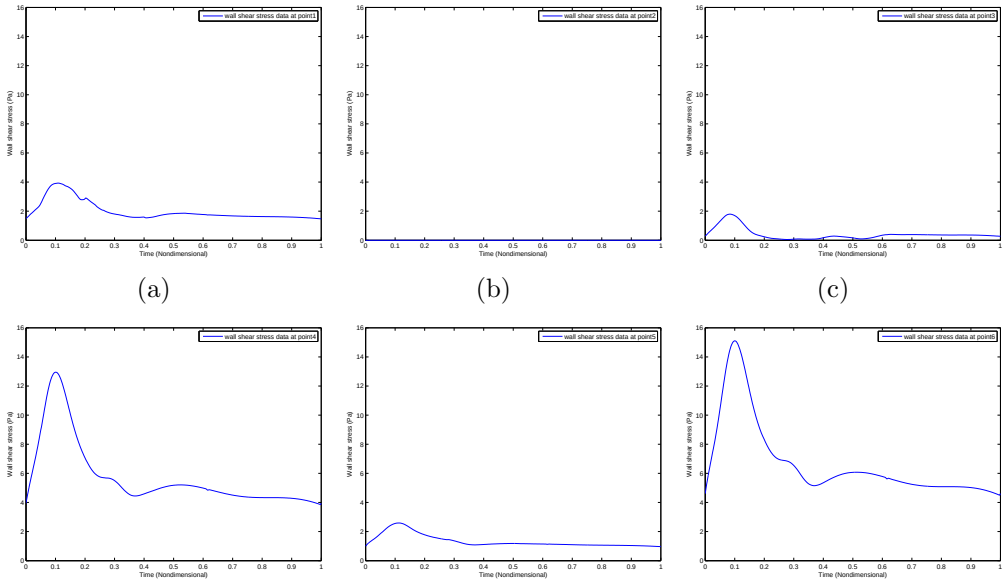

(a) (b) (c)

(d) (e) (f)

Figure 15: The wall shear stress data at the selected six points for one cardiac cycle. The unit of wall shear stress is Pa and the time is given in dimensionless form (by dividing real time by one cardiac cycle time: 0.743 second). Points have different wall shear stress values as shown in the figures a) Point 1, b) Point 2, c) Point 3, d) Point 4, e) Point 5, f) Point 6.

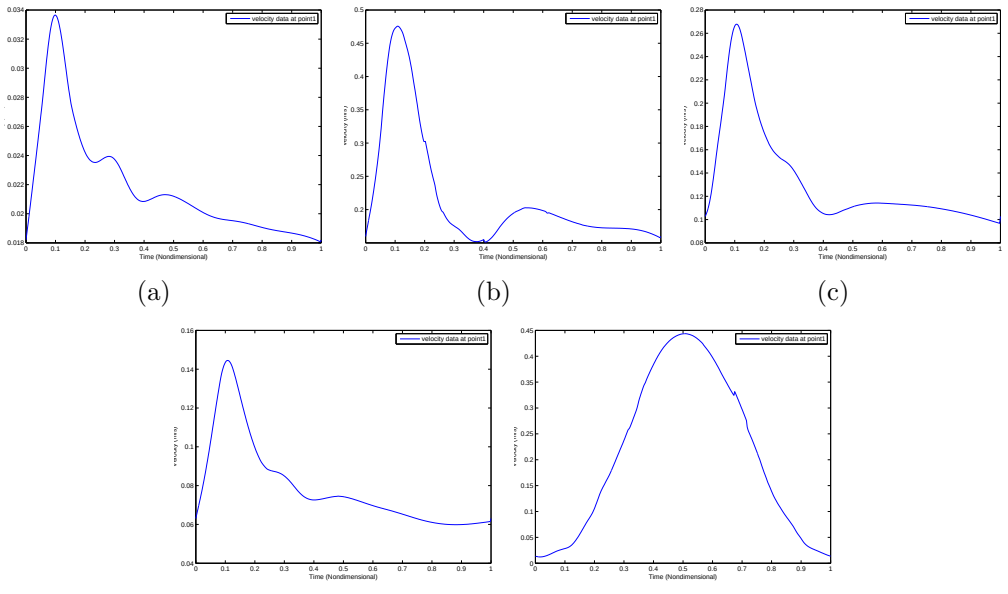

(a) (b) (c)

(d) (e)

Figure 16: The velocity data at point 1 for all cases for one cardiac cycle. The unit of velocity is m/s and the time is given in dimensionless form (by dividing real time by one cardiac cycle time: 0.743 second). Points have different history shape as shown in the figures a) Case a, b) Case b c) Case c, d) Case d, e) Case sinusoidal.

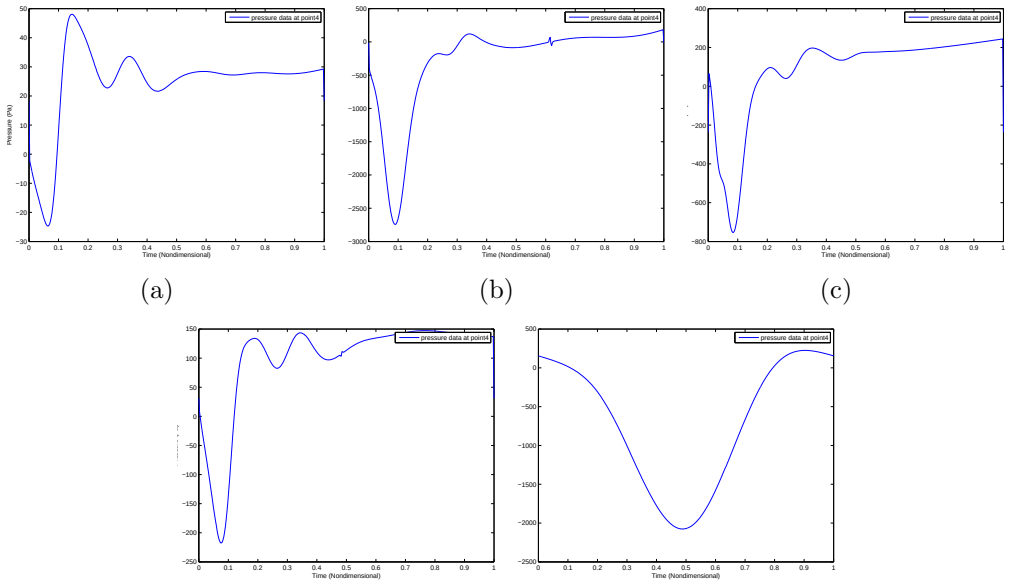

Figure 17: The pressure data at point 1 for all cases for one cardiac cycle. The unit of pressure is Pa and the time is given in dimensionless form (by dividing real time by one cardiac cycle time: 0.743 second). Points have different history shape as shown in the figures a) Case a, b) Case b c) Case c, d) Case d, e) Case sinusoidal.

7 CONCLUSIONS

The numerical simulation of blood flow at carotid artery is investigated in this study. Naturally, one of the most important input of the simulation is the boundary and inlet conditions. Inlet condition for these cases is the Womersley velocity profile which is obtained from experimental data. This study shows that the inlet profile has an important effect on the characteristical behaviour of the blood flow. Changing the velocity inlet does not only change the magnitude of the mechanical properties (pressure, velocity, wall shear stress etc.) but also changes the ordering between points. For low velocity point 3 may have higher velocity than that of point 2 while for high velocity vice versa is possible. Also the pressure drop increases sharply when the inlet velocity increases for points 4 and 6 while it stays constant for other points. Shape of the historical data may change as it can be seen at point 3. These results show that there is highly nonlinear relation between inlet data and characteristics and parameters including pressure, velocity and WSS. This result can be explained or supported by the developement of vortex at especially sinus area and secondary flows because of inflexion regions. Therefore, the eddy developements, secondary flows, and turbulence effects can be investigated as a further study.

8 ACKNOWLEDGEMENT

Computing resources used in this work were provided both by the National Center for High Performance Computing of Turkey (UYBHM) under grant number 20032007

and Istanbul Technical University High Performance Computing Laboratory (BE-YBHM) under grant numbers 5001200300 and 5001200301.

REFERENCES

[1] E. Aribas, S. Piskin, and Celebi M.S. 3d blood flow simulation in human arterial tree bifurcations. In *Proc. of the 14th National Biomedical Engineering Meeting (BIYOMUT 2009)*, Izmir, Turkey, 2009.

[2] L. D. Jou and S. A. Berger. Numerical simulation of the flow in the carotid bifurcation. *Theoretical and Computational Fluid Dynamics*, 10:239–248, 1998.

[3] D. N. Ku. Blood flow in arteries. *Annual Review of Fluid Mechanics*, 29:399–434, 1997.

[4] D. Liepsch. An introduction to biofluid mechanics-basic models and applications. *Journal of Biomechanics*, 35(4):415–435, 2002.

[5] S. Piskin and Celebi M.S. A carotid artery bifurcation model for blood flow. In *Proc. of the 7th Int Symp On Fluid Control, Measurement and Visualization (FLUCOME '03)*, Sorrento, Italy, 2003.

[6] A. Redaelli, F. Boschetti, and F. Inzoli. The assignment of velocity profiles in finite element simulations of pulsatile flow in arteries. *Computers in Biology an Medicine*, 27(3):233–247, 1997.

[7] R. S. Salzar, M. J. Thubrika, and R. T. Eppink. Pressure-induced mechanical stress in the carotid artery bifurcation: A possible correlation to atherosclerosis. *Journal of Biomechanics*, 28(11):1333–1340, 1995.

[8] C.A. Taylors, T.J.R. Hughes, and C.K. Zarins. Finite element modelling of blood flow in arteries. *Computer Methods in Applied Mechanics and Engineering*, 158:155–196, 1998.